Mastering bioactive coatings of metal oxide nanoparticles and surfaces through phosphonate dendrons

Dinh-Vu Nguyen, Ludivine Hugoni, Miriam Filippi, Francis Perton, Da Shi, Emilie Voirin, Laura Power, Geoffrey Cotin, Marie Pierre Krafft, Arnaud Scherberich, et al.

FULL PAPER

Mastering bioactive coatings of metal oxide nanoparticles and surfaces through phosphonate dendrons

Dinh-Vu Nguyen,[a] Ludivine Hugoni,[b] Miriam Filippi,[c] Francis Perton,[a] Da Shi,[d] Emilie Voirin,[a] Laura Power,[c] Geoffrey Cotin,[a] Marie -Pierre Krafft,[d] Arnaud Scherberich,[c] Philippe Lavalle,[b] Sylvie Begin-Colin,[a] Delphine Felder-Flesch*[a]

Abstract: We reported herein an efficient method for constructing dendritic bisphosphonic acid tweezers of generations 1 and 2, which have been proven as versatile surface coatings for metal oxides implant or nanoparticles. These procedures delineated a practical and general route to a library of functional dendrons. Several of these dendritic architectures were successfully tested as biocompatible coverings for iron oxide nanoparticles through *in vitro* assays, but also as antifouling surface coatings for silica through Quartz Crystal Microbalance studies or as stabilizing structure for magnetic nanoparticles-microbubbles conjugates thanks to preliminary Langmuir monolayers studies.

Introduction

Medicine is changing.[1] New technologies are revolutionizing therapeutic treatments, in various domains such as preventive medicine or diagnosis, [2] management of diseases or medical implants.[3] A multidisciplinary research at the interface of materials and surface chemistry, biology, physics and medicine paves the way to a new era, in which innovative strategies could strongly improve early diagnosis of diseases, patientsô comfort, with reduced intervention time and an unprecedented efficiency.
Applications of nanoscience and nanotechnologies to biomedical and clinical purposes raise then strong expectations, [4] especially in three specific medical domains, namely: early diagnosis, [5] targeted drug delivery [6] and regenerative surgery. [7]
Indeed, throughout the last decades, the development of nanosized objects has gathered significant attention from the scientific community. [8] For instance, in the field of medical imaging, many techniques (radiography, magnetic resonance imaging (MRI), scintigraphy, echography) could be implemented by the use of so called *theranostic objects*, [9] namely materials capable of combining diagnostic and therapeutic activity in one single platform. However, early diagnosis and effective treatment are not the only challenges that nanoscience may address. Indeed, many devices dedicated to medical implantation require robust surfaces [10] whose properties do not change over time, and in this regards, simple and effective solutions are still being sought by manufacturers. Moreover, the development of smart surfaces to avoid microbial colonization is also necessary, [11] for instance for engineering cardiac valves. It is therefore imperative to develop innovative strategies based on nanotechnologies in order to prevent infections related to implanted materials, facilitate diagnosis and improve patientsôcare.
For such utilities, an efficient organic coating is highly essential to modulate the nanomaterialsôproperties. [12] In this perspective, the dendritic approach has been proven versatile thanks to the precisely defined structure and composition as well as the enhanced tunable surface chemistry of those arborescent architectures. [13]
Thus, using a multifunctional approach based on the chemistry of dendritic macromolecules, we aim at meeting the challenges of early diagnosis of diseases and follow-up of implant placement. As these preliminary results show, this multifunctional approach enables to obtain a nanomedicine tool of nanoparticle (NP), implant or microbubble (MB)-type, endowed with increased *in vivo* stability, reduced toxicity as well as antifouling properties.

Results and Discussion

Preparation of starting building blocks

Scheme 1 depicts the preparation of common building blocks that are used iteratively. Tosyl azide **15** is representative for the ethylene unit spacer between each generation (G) of dendron. It was obtained in two steps from 2-Bromoethanol, first by substitution of the bromine atom with sodium azide, then activation of the primary alcohol **14** with tosyl chloride. **15** was

[a] Dr. D.-V. Nguyen, F. Perton, E. Voirin, Dr. G. Cotin, Dr. S. Begin-Colin, Dr. D. Felder-Flesch
Institut de Physique et de Chimie des Matériaux de Strasbourg
IPCMS UMR CNRS UNISTRA 7504
23 rue du loess BP 43 67034 Strasbourg cedex 2, France
E-mail: Delphine.Felder@ipcms.unistra.fr
[b] L. Hugoni, Dr. P. Lavalle
INSERM UMR 1121, Biomaterials and Bioengineering
Université de Strasbourg, 11 rue Humann, 67000 Strasbourg, France
[c] Dr. M. Filippi, L. Power, Dr. A. Scherberich
Department of Biomedicine, University of Basel, University Hospital Basel, Hebelstrasse 20, 4031, Basel, Switzerland.
[d] Dr. M. P. Krafft, D. Shi
University of Strasbourg
Institut Charles Sadron (UPR 22, CNRS)
23 rue du Loess. 67034 Strasbourg Cedex (France)

Supporting information for this article is given via a link at the end of the document.

next linked to the phenol **16** [14] in a basic medium to afford the bisphosphonate **17** in 82% yield in three grams scale. Different oligoethylene glycol (OEG) chains were used to functionalize the library of dendrons. They were first converted into tosylate (**18** to **21**), then Filkelstein reaction allowed to obtain OEG with an iodide as leaving group (**22** to **25**).

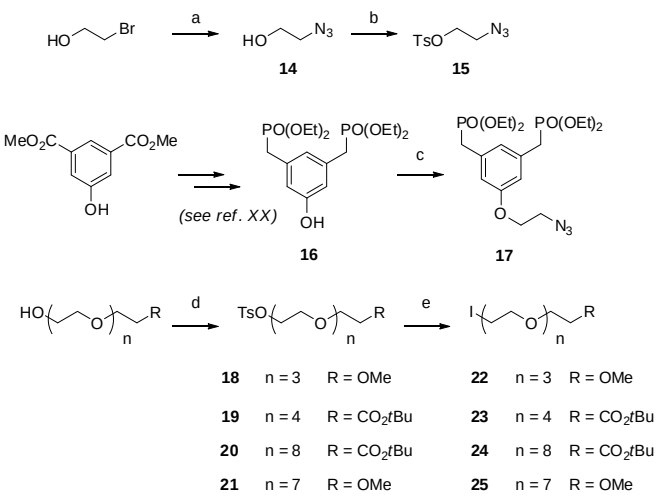

Scheme 1. Preparation of starting building blocks. (a) NaN_3, H_2O, 75%; (b) TsCl, Et_3N, CH_2Cl_2, 76%; (c) KOH, KI, **16**, DMSO, 82% ; (d) TsCl, Et_3N, CH_2Cl_2, 82% for **18**, 81% for **19**, 99% for **21**, 99% for **20**; (e) KI, Acetone, 94% for **22**, 96% for **23**, 99% for **24**, 89% for **25**.

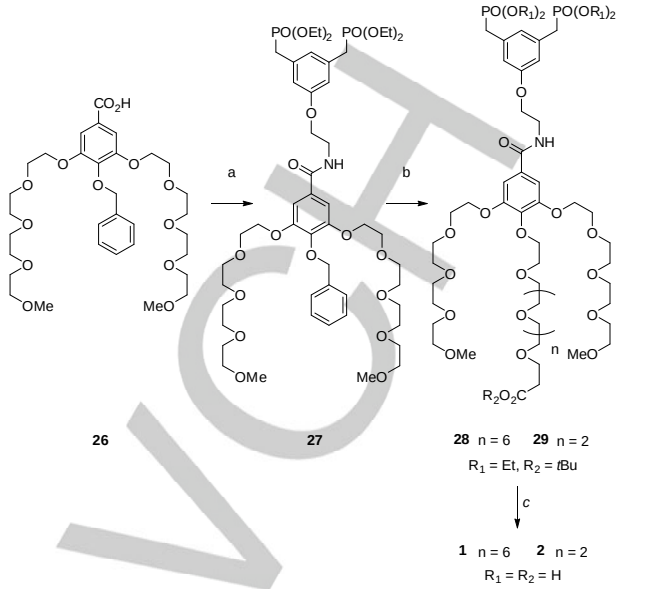

Scheme 2. Synthesis of bisphosphonic acids of first generation **1** and **2**. (a) **17**, Pd/C, H_2, EtOAc then **26**, $(COCl)_2$, DMF, DIPEA, CH_2Cl_2, 79%; (b) H_2, Pd/C, EtOAc, then K_2CO_3, KI, **19** (or **20**), 96% for **28**, 94% for **29**; (c) TMSBr, CH_2Cl_2, 90% for **1**, 94% for **2**.

Part 1: Development of dendritic coatings for implant surfaces

The first event during implantation of a biomaterial in the body is protein adsorption. This process can be the starting point of the foreign body reaction which leads to tissue encapsulation of the biomaterial.[15] The design of efficient antifouling surface is thus of primary interest when an implant is currently concerned by this type of phenomenon. Moreover such antifouling coatings can also limit the risk of infections and formation of biofilms which is a major issue for many implants.[16]

We have previously reported the synthesis of the Gallate based bisphosphonates decorated with multiple OEG side chains.[14] In the course to the development of dendritic coatings for biomedical devices, these syntheses were thoroughly revised in order to generate a library of dendrons with an enhanced robustness. The synthesis of dendrons of first generation (G1) is similar to the one reported in the literature, except that azide function was selected as the latent amine. Thus the key amide coupling was conducted after two separate steps: i) generation of the corresponding amine from azide **17** by hydrogenation, ii) formation of acyl chloride from the carboxylic acid **26** [14] with oxalyl chloride and a catalytic amount of DMF. The key intermediate **26** obtained in four grams scale (79%) was carried to the known bisphosphonic acids **1** and **2** following our previously reported procedure (Scheme 2).[14]

The bisphosphonic acid **1** was primarily evaluated by biologist partners for the antimicrobial and antifouling properties. Although OEG is known as an efficient mean to prevent the nonspecific protein adsorption,[17] we sought to improve this ability by functionalizing the surface with molecules displaying antifouling properties, e.g. polycationic or zwitterionic molecule. This chemisorption is achieved via an amide coupling between the carboxylic acid group of **1** and the amine group in the biomolecule. Alternatively, the physical adsorption was also considered.

The synthesis of model bisphosphonic acid **3** with three similar and unfunctional OEG side chains is depicted in Scheme 3. First Methyl gallate was fully functionalized with OEG **18** to afford methyl ester **30** which was transformed by a saponification into its carboxylic acid analog **31**. The amide coupling with **17** was accomplished with EDCI and a catalytic amount of DMAP, and the final deprotection of phosphonate groups with trimethylsilyl bromide (TMSBr) afforded the desired model compound **3.**

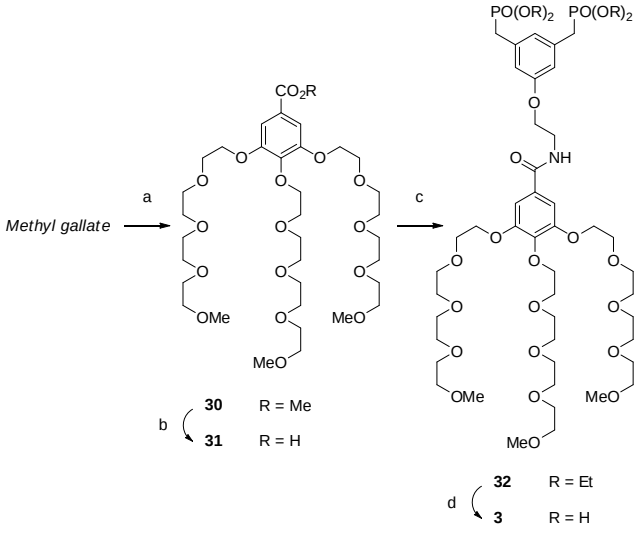

Scheme 3. Synthesis of bisphosphonic acid of first generation **3**. (a) K_2CO_3, **18**, Acetone, 87%; (b) NaOH, MeOH/H_2O, 99%; (c) **17**, Pd/C, H_2, EtOAc then EDCI, DMAP, CH_2Cl_2, 86%; (d) TMSBr, CH_2Cl_2, 90%.

Dendron of second generation (G2) required an additional 3,5-Dihydroxybenzoic acid methyl ester as connector (Scheme 4). Its synthesis began with double functionalization of this latter with tosyl azide **15**, followed by saponification to afford carboxylic acid **34** in 83% overall yield. Then, amide coupling with azido **17**, upon hydrogenation, yielded bisphosphonate **35** in 98% yield in two grams scale.

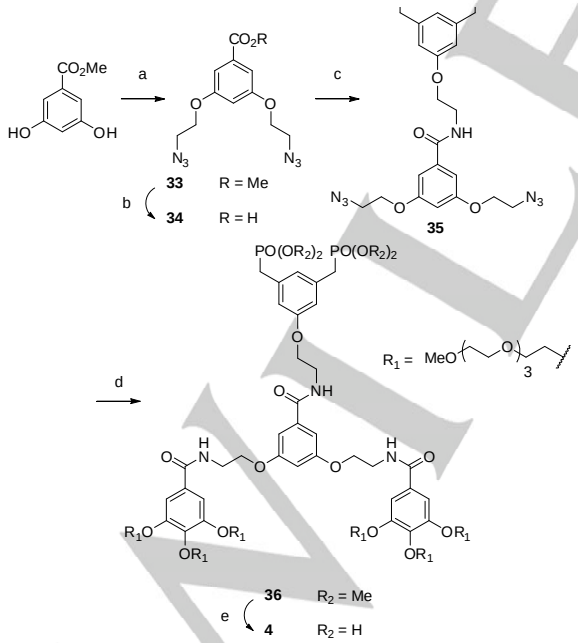

Scheme 4. Synthesis of bisphosphonic acid of second generation **4**. (a) **15**, KOH, KI, DMSO, 87%; (b) NaOH, MeOH/H_2O, 95%; (c) **17**, Pd/C, H_2, EtOAc then EDCI, DMAP, CH_2Cl_2, 98%; (d) Pd/C, H_2, MeOH then **31**, EDCI, DMAP, CH_2Cl_2, 81%; (e) TMSBr, CH_2Cl_2, 73%.

Access to G2 model dendron **4** was secured in the following strategy: i) double hydrogenation of **35** catalyzed by Pd/C, ii) amide coupling with carboxylic acid **31** by using EDCI and a catalytic amount of DMAP, iii) removal of ethylphosphonate with TMSBr.

Regarding functionalized G2 dendrons (Scheme 5), a similar synthetic pathway than G1 counterparts was used. Bis-azide **35** reacted with carboxylic acid **26** to provide the key intermediate **37** in one-gram scale. At this stage, only two last steps are required to complete the synthesis: i) removal of the benzyl group, ii) *O*-alkylation to introduce the middle OEG side chain. Nevertheless, several challenges are involved in these simple transformations. First, the increased density of OEG might sequester the metal for the heterogeneous hydrogenation, thus significantly hampering the debenzylation step. Second, upon removal of the benzyl group, *O*-alkylation in the middle position of the Gallate moiety could suffer from steric issue. With those potential problems in mind, we first used the classical condition, *i.e.* Palladium on charcoal for the hydrogenolysis, then alkylation of OEG **19**-**21** with K_2CO_3/KI (cat.) in reflux of Acetone. Unfortunately, none of these conditions were successful. We finally learned that a two-step procedure involving hydrogenolysis with Pearlman's catalyst in MeOH and subsequent *O*-alkylation with OEG bearing an iodide as leaving group (**23** to **25**) in DMF were the key for the success outcome of this last step. As an example dendron **39** was thus isolated in 73% yield (over 2 steps) in half-gram scale. The final deprotection with TMSBr in reflux of Dichloromethane afforded a series of dendron **5** to **7**.

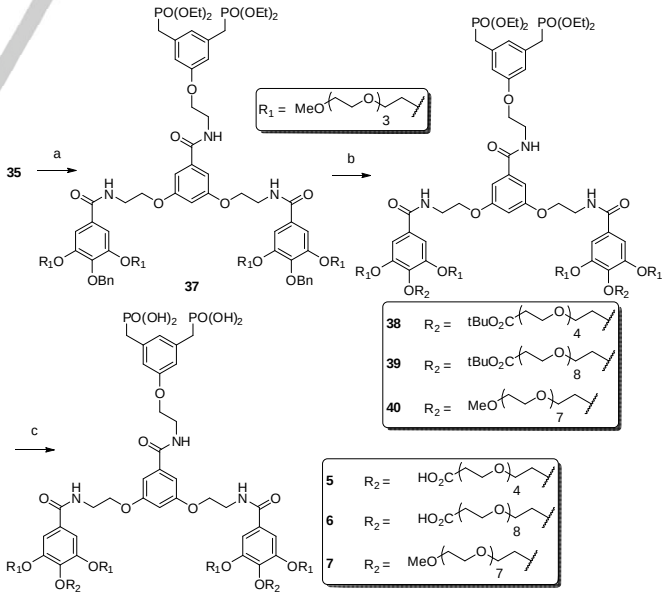

Scheme 5. Synthesis of bisphosphonic acids of second generation **5**-**7**. (a) H_2, Pd/C, MeOH, then **26,** EDCI, DMAP, DMF, 61%; (b) H_2, $Pd(OH)_2$/C, MeOH,

then **23**-**25**, K_2CO_3, DMF, 73% for **38**, 73% for **39**, 44% for **40**; (c) TMSBr, CH_2Cl_2, 68% for **5**, 71% for **6**, 60% for **7**.

The last dendron **8** belonging to the G2 series exhibits a full coverage of functional octaethyleneglycol side chain (Scheme 6). The notable issue implied the compatibility of *tert*-butyl ester group toward the acidic or basic condition reported throughout the synthetic pathway (vide supra). As a result, Methyl gallate was substituted by Benzyl gallate whose deprotection can be chemoselectively conducted by hydrogenolysis in the presence of *tert*-butyl ester. The introduction of OEG side chain in the *para* position was first accomplished with $KHCO_3$/DMF and OEG **24** having an iodide as leaving group, then two equivalents OEG **20** were subsequently added by using K_2CO_3 in reflux of Acetone. In this manner, the isolated yield was significantly improved, whilst the one-pot trisubstitution of Benzyl gallate surprisingly ended to the decomposition of starting materials. With compound **42** in hand, coupling with bis-azide **35** could be successfully executed under HATU/DIPEA conditions after removal of the Benzyl group by hydrogenation. Despite a full conversion determined by ^1H NMR analysis of the crude product, **44** was only isolated in an un-optimized yield of 59% after a reverse phase chromatography purification step. Finally, the concomitant deprotection of phosphonate and carboxylic groups with TMSBr afforded phosphonic acid **8**.

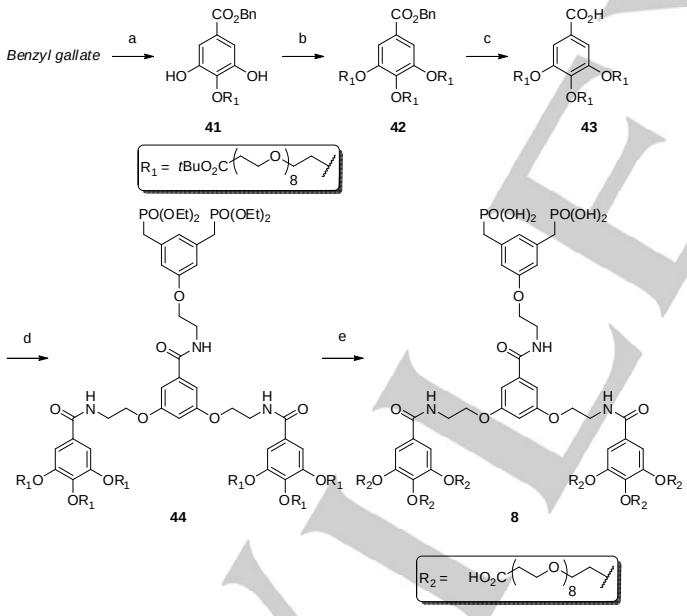

Scheme 6. Synthesis of bisphosphonic acid of second generation **8**. (a) $KHCO_3$, **24**, DMF, 88%; (b) K_2CO_3, KI, **20**, Acetone, 80%; (c) H_2, $Pd(OH)_2/C$, MeOH, 93%, (d) **35**, H_2, Pd/C, MeOH, then HATU, DIPEA, DMF, 59%, (e) TMSBr, CH_2Cl_2, 67%.

Quartz Crystal Microbalance preliminary studies on SiO_2

In order to characterize the dendritic coatings on oxide surfaces, Quartz Crystal Microbalance with Dissipation monitoring (QCM-D) experiments were performed with dendrons **2** to **7**. In order to highlight the importance of the molecular design, these latter were classified by generation and by the OEG peripheral derivatization, *i.e.* **2** versus **3**, **4** versus **5**, and **6** versus **7** (Figure 1).

The kinetics of mass deposition on SiO_2 crystals showed quasi-steady state after 30 min of dendron injections, which could be related to surface saturation. After rinsing with pure water, a weak desorption was observed reaching rapidly a steady state (å3min) indicating a strong anchoring of the dendrons on the surface. Figure 2 summarizes the density of the dendrons deposited on SiO_2 surfaces after the rinsing steps. Concerning dendron **2** and **3**, the mass adsorbed on the surface reached about 200 ng/cm². This density was about 2-fold higher for the other dendrons, reaching about 400 ng/cm² for **4** to **7**, which correspond to G2 dendrons.

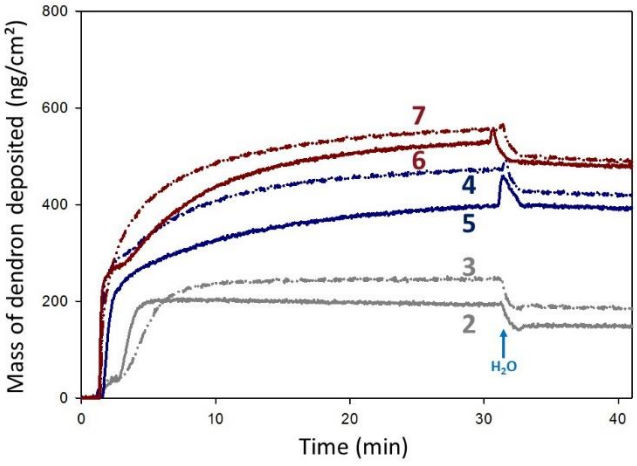

Figure 1. Kinetic of dendrons **2** to **7** deposition on SiO_2 quartz crystal (ng/cm²) evaluated by Sauerbrey's modeling from QCM-D analysis (based on the variations of resonance frequency of 3/3, for 3 = 3). Rinsing with H_2O was applied after 31 min deposition. Experiment was repeated three times.

Finally, in terms of mass density, lower amounts of G1 (**2** and **3**) than G2 dendrons (**4** to **7**) were deposited on the surface. However, taking into account their respective molecular weight, it appears that 10^{14} molecules.cm^{-2} were deposited on the surfaces whatever the dendron. In other words, the increase of mass density observed for G2 dendrons **4** to **7** is related to their macro-architecture: their greater bulkiness allows a more flexible conformation to be packed on the surface. Furthermore, the nature of their chemical end groups, -COOH or -OMe, does not influence the kinetic of deposition and final amount adsorbed, indicating that the adsorption on the SiO_2 surface is probably mediated through the phosphonate tweezers as expected.[18]

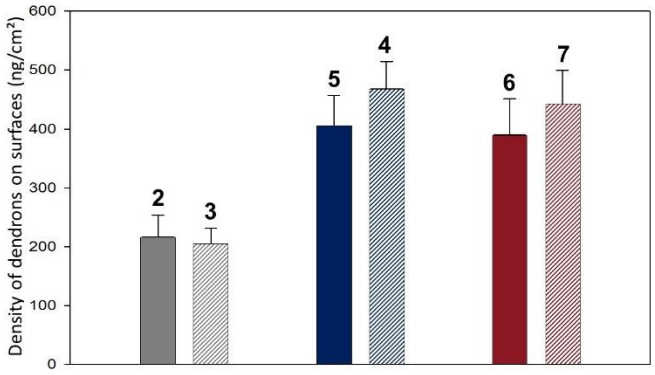

Figure 2. Density of dendrons **2** to **7** on SiO_2 quartz crystal (ng/cm²) evaluated by Sauerbrey's modeling from QCM-D analysis (based on the variations of resonance frequency of 3/3, for 3 = 3). Each values corresponds to the mean value of three measurements performed on three samples and error bars correspond to standard deviations.

Regarding the antifouling properties of the dendron-coated surfaces, 10 % fetal bovine serum (FBS) were injected in order to further analyze the serum protein adsorption by QCM-D (Figure 3). The results indicated that the dendritic coatings provide an antifouling character when compared to bare surfaces: 974 ± 19 ng/cm² of serum protein were adsorbed on bare SiO_2 *vs* 739 ± 30 ng/cm² for G1 (**2** and **3**), 435 ± 29 ng/cm² and 360 ± 141 ng/cm² for G2 coated surfaces. Note that the coatings made from G2 dendrons (**4** to **7**) show more than a 2-fold lower protein adsorption than bare SiO_2 whereas G1 dendron only reduced by about 24% the protein amount adsorbed. Such trend could be explained by the presence of a higher density of OEG chains in the G2 structures which is known to prevent protein adsorption.[17] Finally, G2 dendron **4** is the most efficient to prevent protein adsorption (reduction of about 75%) making it a promising candidate for surface functionalization.

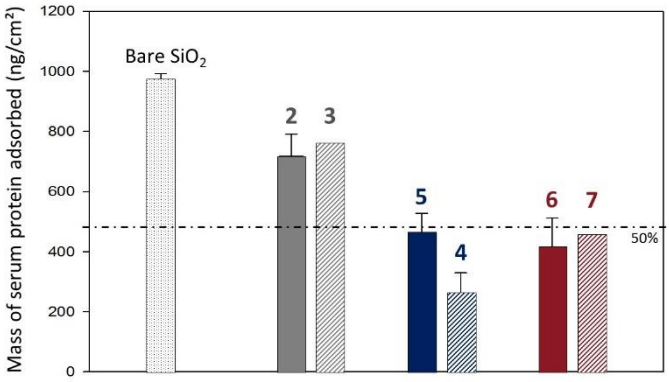

Figure 3. Mass of serum protein adsorbed on dendron-coated SiO_2 quartz crystal (ng/cm²) evaluated by Sauerbrey's modeling from QCM-D analysis (based on the variations of resonance frequency of 3/3, for 3 = 3). Values are mean ± SD. Each values corresponds to the mean value of three measurements performed on three samples, and error bars correspond to standard deviations.

Part 2: Development of dendritic coatings for metallic oxide nanoparticles

Research on inorganic nanoparticles (NPs) is rapidly expanding with a large variety of applications, as well as strategies for their synthesis. [19] Most often, the surface modification of the NPs is crucial, in particular to avoid their aggregation, make them dispersible in liquid media or derivatize them with functional end groups for further modification with targeting ligands or other bioactive molecules. Here again, the exceptional binding properties of phosphonic acids to oxide surfaces have attracted much attention, such that many examples of decorated magnetic metal oxide NPs using phosphonate terminated molecules have recently emerged in the literature. [20]

Many research groups worldwide are actively developing superparamagnetic iron oxide (SPIO) NPs leading to a vast number of applications in health sciences, including for example combined *in vivo* MRI and optical imaging (OI) via multimodal NPs based on fluorescent probes conjugated to SPIO NPs, [21] hyperthermia heating of tumour,[22] and drug delivery. [23] In this context, biofunctionalization of NPs is most often required to avoid aggregation or rapid clearance by the Mononuclear Phagocyte System (MPS).[24]

The evaluation of tumor perfusion and oxygenation status is very important in oncology since tumor hypoxia appears to be strongly associated with propagation, malignant progression, and resistance to therapy.[25] It is therefore important to develop efficient probes to perform *in vivo* imaging of the hypoxic tissue in order to increase the therapeutic efficacy in these resistant hypoxic cells.[26] Bioreductive compounds, which are selectively reduced in hypoxic tissue to reactive intermediates that bind to intracellular molecules, have been used for targeting hypoxic tumors. Even though also other functional groups in this category (such as nitroaromatics and N-oxides) have been extensively studied, the nitroimidazole is one of the preferred pharmacophores to develop probes for tumour hypoxia detection.[27] Indeed, under hypoxic conditions, a reduction step on the nitro group occurs and the so-derived moieties covalently bind to intracellular macromolecules. With this in mind, we decided to derivatize our bisphosphonic acids with Metronidazole groups.

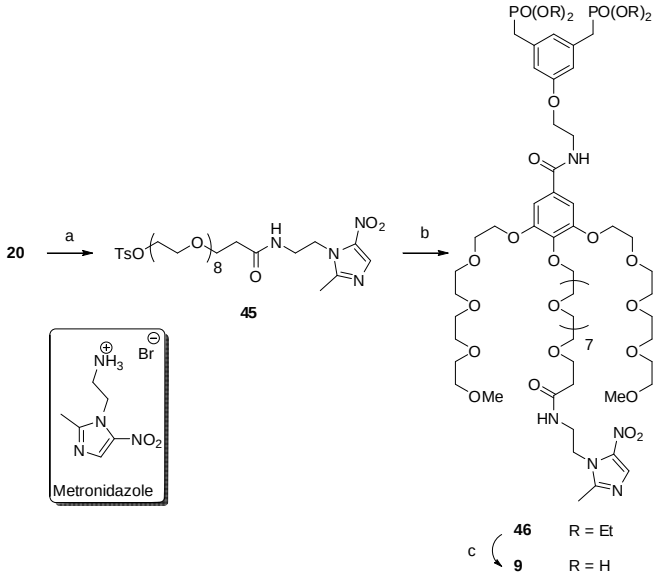

Scheme 7. Synthesis of bisphosphonic acid with one metronidazole group **9**. (a) TFA, CH_2Cl_2, then $(COCl)_2$, DMF, CH_2Cl_2, then Metronidazole, DIPEA, CH_2Cl_2, 56%; (b) **27**, Pd/C, H_2, EtOAc then K_2CO_3, KI, Acetone, 86%; (c) TMSBr, CH_2Cl_2, 81%.

Our route to metronidazole-functionalized dendron **9** started with the preparation of the functional OEG **45** (Scheme 7). The metronidazole, prepared according to known procedure,[28] was linked to OEG **20** via the formation of the corresponding acyl chloride. The functionalization of key intermediate **27** with the resulting OEG **45** was accomplished using strategy described in scheme 7: upon hydrogenation of **27** with Pd/C, *O*-alkylation with **45** by using K_2CO_3 and KI in reflux of Acetone produced bisphosphonate **46** in 86% yield. The final deprotection with TMSBr provided cleanly phosphonic acid **9**.

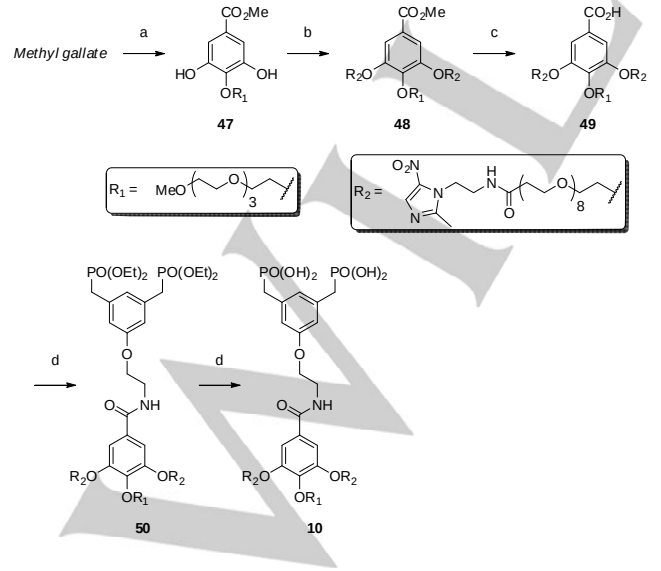

Scheme 8. Synthesis of bisphosphonic acid with two metronidazole groups **10**. (a) $KHCO_3$, **22**, DMF, 86%; (b) K_2CO_3, KI, **45**, DMF, 88%; (c) NaOH, $MeOH/H_2O$, 99%; (d) **17**, Pd/C, H_2, EtOAc, then EDCI, DMAP, CH_2Cl_2, 37%; (d) TMSBr, CH_2Cl_2, 72%.

Taking advantage of the multiple OEG arms on the dendritic structures, we introduced additional hypoxic markers as shown in scheme 8 with a slight modification compared with the access to mono-functionalized dendron **9**: Methyl gallate was first functionalized in *para* position with OEG **22** with $KHCO_3$ in DMF, followed by two OEG chains **45** with K_2CO_3 in DMF. The purification by C_{18} reverse phase chromatography was necessary from this stage to obtain satisfactory yields. Then saponification of **48** provided carboxylic acid **49**, which reacted with phosphonate **17** using EDCI in the presence of catalytic amount of DMAP to provide dendron **50** in 37% yield overall yield. Final deprotection with TMSBr afforded phosphonic acid **10**.

Synthesis of dendronized NP@metronidazole

IO NPs with a mean diameter of 9.0 ± 0.9 nm were synthesized by thermal decomposition of Iron (II) stearate in the presence of oleic acid (OA) in dioctyl ether.[29] The functionalization of the NPs was performed by direct ligand exchange in THF for 24 h and the excess of dendron was removed by ultrafiltration. In order to investigate the influence of the metronidazole group on the physico-chemical properties of dendronized NPs, various weight ratio of dendrons **9** and **1** (1/0, 75/25, 50/50, 25/75, 0/1 w/w **1**:**9**) were grafted on the surface of the NPs. The functionalization was assessed by Dynamic Light Scattering (DLS) measurements and by infrared spectroscopy (IR) (see ESI) showing the disappearance of the OA alkyl bands (2926-2850 cm^{-1}) and the appearance of the OEG characteristic signal (1096 cm^{-1}). High resolution magic angle spinning (HR-MAS) ^1H nuclear magnetic resonance (NMR) was also performed to assess the presence of **9** (see ESI). As shown by DLS (Figure 4), the colloidal stability was preserved for all ratio. A slight shift in hydrodynamic diameter was observed with the increasing ratio of **9**, which can be attributed to the longer middle OEG chain.

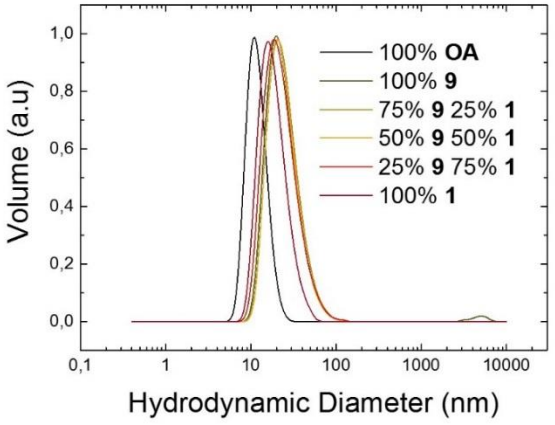

Figure 4. Dynamic light scattering (DLS) measurements in pure water (pH 7) performed on dendronized NPs of various ratios of **1**:**9**. OA: oleic acid.

Effects of Metro-NPs on the viability and proliferation of cells grown on monolayer

In the perspective of their potential use for biomedical applications, the impact of the dendronized NPs@**9** on cell viability was assessed on human umbilical vein endothelial cells (HUVEC) grown on monolayer and exposed to different nanomaterial concentrations for various time durations. The NPs displayed a high level of biocompatibility; with short incubation times and low NP dosages, viability was always above 80% (Figure 5 and ESI), and even in the harshest conditions, namely the combination of the longest incubation time (two days) and the highest dosage (150 µg Fe/mL), the viability only dropped by 20%. The effects induced by the functional NPs were not substantially different from those caused by the control NPs@**1**.

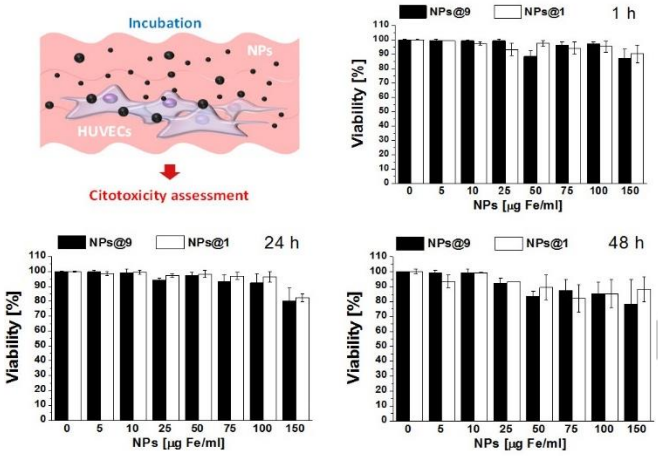

Figure 5. Effects of NPs@**9** and NPs@**1** on cell viability. Viability of HUVEC cells after incubation at 37 °C with different dosages of functionalized NPs@**9** and un-functionalized NPs@**1** nanoparticles for various time ranges, as tested by MTT assay.

US and MRI, a valued strategy for improving the accuracy of diagnosis.[34]

For the synthesis of fluorinated dendrons, the piperazine scaffold was selected as template to introduce the perfluoro side chain. It was installed by using HATU as coupling agent, upon a careful deprotection of **28** in acidic condition (Scheme 9). At this point, removal of the protecting group by simple hydrogenolysis of **51** afforded the secondary amine, ready to react with the requisite perfluoroalkyl iodide. This sequence allowed to produce bisphosphonates **52**-**54** in reasonable yield (55 to 80%), despite their high polarity. The synthesis was achieved by the usual deprotection of phosphonate group with TMSBr to generate bisphosphonic acids **11**-**13**.

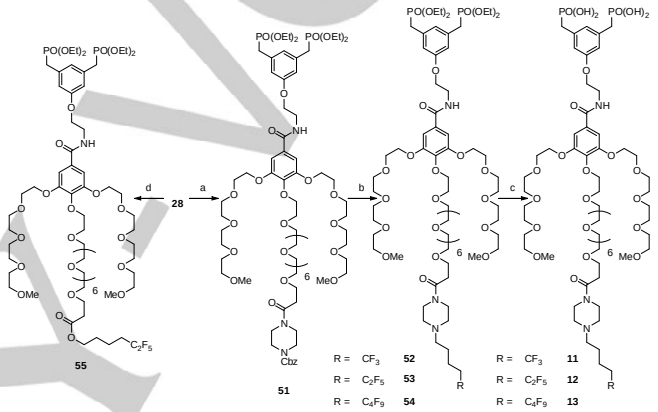

Scheme 9. Synthesis of bisphosphonic acid **11**-**13** used to coat iron oxide nanoparticles. The dendronized nanoparticles are intended to be used in combination with phospholipids to form the shell of hybrid microbubbles. (a) TFA, CH_2Cl_2, then piperazine-NCbz, HATU, DIPEA, DMF, 99%; (b) H_2, Pd/C, MeOH, then perfluoroalkyliodide, K_2CO_3, CH_3CN, 62% for **52**, 80% for **53**, 55% for **54**; (c) TMSBr, CH_2Cl_2, 78% for **11**, 79% for **12**, 80% for **13**; (d) TFA, CH_2Cl_2, then 1,1,1,2,2-pentafluoro-6-iodohexane, K_2CO_3, CH_3CN, 92%.

Part 3: Dendritic coatings for the development of hybrid microbubbles

Soft-shell (*e.g.* lipid-shell) microbubbles (MBs) are ideal soundwave reflectors, and several fluorocarbon-stabilized MB formulations are commercially available for diagnostic ultrasound (US) imaging.[30] MBs are also being involved in several applications including molecular imaging, surgical ablation, targeted drug and gene delivery.[31] In particular, they have been extensively used in conjunction with focused US and under MRI guidance, in order to achieve blood/brain and blood/tumor barrier crossing of drugs.[32] NPs can be attached to the MBs to extend their theranostic potential by combining multimodal imaging, drug or gene delivery, and/or enhancement of the acoustic signal. Magnetic MBs have been reported.[33] Taking advantage of the high colloidal stability of IO NPs when dendronized, we have designed MBs stabilized by combination of phospholipids and dendronized IO NPs. Various dendrons, some of which are fitted with fluorinated end groups (Scheme 9) were investigated. These MBs constitute potential bimodal contrast agents to be used for

In order to rationalize the design of phospholipid-based MBs fitted with dendronized NPs in their shell, it was essential to first investigate the ability of mixtures of phospholipids and dendrons to form stable Langmuir monolayers at the air/water interface. The compression isotherms of monolayers of dimyristoylphosphatidylcholine (DMPC), dendron labeled with a C_2F_5 end group, **55**, and of a DMPC/dendron mixture (75:25 in molar ratio) are shown in Figure 6. The pressure/area isotherm of DMPC is monotonous, reflecting the liquid-expanded character of the monolayer throughout compression. By contrast, the isotherm of the dendron shows a transition at a surface pressure σ of ~15 mN m^{-1} and a molecular area A of ~350 $Å^2$. This transition can be assigned to the progressive solubilization of the OEG chains of the dendron in the aqueous sub-phase, which leads to the collapse of the monolayer at σ ~32 mN m^{-1}. The presence of the dendron in the mixed monolayer is evidenced by the shift in σ for A larger than ~70 $Å^2$. For A < 70 $Å^2$, the isotherm of the mixed monolayer is nearing that of the DMPC monolayer, reflecting progressive expulsion of the dendron, either by solubilization in the sub-phase or growth of 3D aggregates in the monolayer. The mixed DMPC/dendron monolayers were transferred on silicon

wafers using the Langmuir Blodgett method, and analyzed with atomic force microscopy (AFM) in order to provide insights on their composition and morphology. When transferred at ~14 mN m^{-1}, that is, before the onset of the transition, domains of dendrons (170 ± 20 nm in size, ~1.2 nm in height) can be observed. These domains are embedded in the DMPC monolayer, and, occasionally a 3D crystal of dendron is detected (Fig. 6B). When the pressure of transfer is increased to 30 mN m^{-1}, significantly more numerous and larger chains of dendron crystals (~4.0 nm in height) are seen.

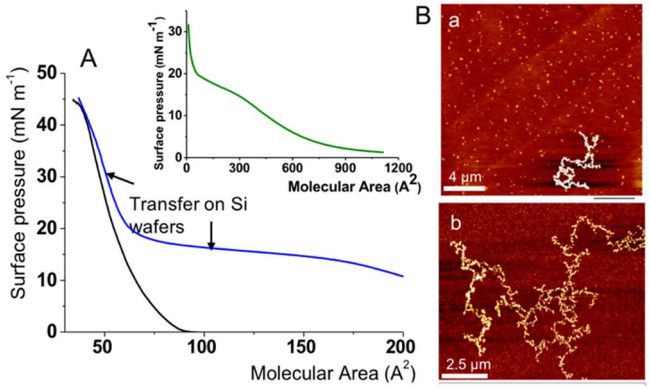

Figure 6. A) Compression isotherms at 25°C of Langmuir monolayers of DMPC (black), and DMPC/dendron **55** (75:25 molar ratio; blue). Inset: isotherm of the fluorinated dendron **55** alone (green) and. B) atomic force micrographs of Langmuir monolayers of the DMPC/dendron **55** mixture after transfer on silicon wafers at a) 14 mN m^{-1} and b) 30 mN m^{-1}.

These investigations provide the guidelines needed to prepare stable DMPC monolayers that incorporate dendrons. These results show that small domains of dendrons can be accommodated in the phospholipid monolayer as long as the surface pressure remains below the collapse pressure of the dendron. The latter can be controlled by adjusting the dendron structure, in particular by changing the length of the hydrophobic group at the end of the longest OEG chain. This opens new perspectives for synthesizing dendrons specifically adapted for the introduction of dendronized nanoparticles in the phospholipid shells of theranostic MBs as bimodal contrast agents for US and MR imaging.

Conclusions

We have reported the synthesis of a library of dendritic bis phosphonic acids. The practical protocols and robustness were also demonstrated as two of them (dendrons **1** and **4**) were prepared in a gram scale with high synthetic yields. Moreover, a selection of them was also successfully grafted onto IO NPs or MBs surface as well as on flat silica surfaces. Surface pressure/molecular compression isotherms of DMPC/dendron mixed Langmuir monolayers were investigated, providing guidelines in the production of MBs fitted with dendronized NPs to be used both for US and MRI. Currently, our main objective is to bring these hybrid nanomaterials to a step further with assessment of their stability in physiological medium and biological *in vivo* studies.

Experimental Section

Preparation of dendritic building blocks (See ESI)

Quartz crystal microbalance with dissipation monitoring (QCM-D)

Dendritic coatings were deposited on SiO_2 quartz crystal sensors (QSX 303, Qsense®, Biolin Scientific AB, Sweden) and further analyzed using a quartz crystal microbalance with dissipation monitoring (QCM-D, E1 Qsense®, Biolin Scientific AB, Sweden). Firstly, bare SiO_2 crystals were excited at their fundamental resonance frequency (ɜ = 0, corresponding to 5 MHz) at T = 25 °C and the variations of resonance frequency were measured at the first four odd overtones (noted ī qƒɜ with ɜ = 3, ɜ = 5, ɜ = 7 and ɜ = 9 corresponding to 15, 25, 35 and 45 MHz, respectively). To perform the deposition, 400 µL of dendrons (1 $mg.mL^{-1}$ in pure water) such as **2**, **6** or **5**, with -COOH or -OMe end groups, were loaded in the sensors for 30 min and rinsed with 400 µL H_2O MilliQ® for 10 min at T = 25 °C. After dendron deposition, Sauerbreyȭs modeling was used to determine the mass adsorbed on the crystal surfaces. Sauerbrey approximation can be used as the normalized frequency shifts for the various overtones display almost identical values and slight shifts in dissipation were monitored. [35]

Characterization of antifouling properties

Following dendron deposition on the SiO_2 crystal surfaces, 400 µL buffer containing 10 mM of Tris(hydroxymethyl)-aminomethane (TRIS) (Merck, Germany) and 150 mM NaCl (Fisher Scientific, France) at pH 7.4 were injected for 10 min in the sensor. 400 µL of fetal bovine serum (FBS, S1810 Dutscher, France) diluted at 10 % (v/v) in the Tris-NaCl buffer were deposited on the dendron-coated surfaces for 30 min. Then a flow of Tris-NaCl buffer (250 $µL.min^{-1}$) rinsing solution was continuously applied during 200 min. Finally, serum protein adsorption was evaluated by Sauerbreyȭs approximation.

Synthesis and functionalization of iron oxide nanoparticles

10 nm spherical nanoparticles were synthesized by thermal decomposition. Briefly, iron II stearate (2.2 mmol), oleic acid (4.4 mmol) and dioctyl ether (20 mL) were mixed together in a 100 mL two necked round bottom flask. The mixture was magnetically stirred for 1 h at 100 °C to remove the excess of water. Then the solution was heated under reflux to the boiling point of the dioctyl ether for 2 h without any stirring. The solution was purified six times by centrifugation (14000 rpm, 5 min) with a mixture of chloroform/acetone (v/v 1:5).

In a 30 mL vial, a suspension of nanoparticles in 5 mL THF (5 mg of iron) was introduced together with 7 mg of the desired mixture of dendrons and the vial was completed with 10 mL of THF. The mixture was magnetically stirred for 24 h, then the particles were centrifuged, re-dispersed in water and washed by ultrafiltration.

Cell lines

Human umbilical vein endothelial cells (HUVEC) were obtained from American Type Culture Collection (ATCC, Manassass, VA, USA) and were tested for mycoplasma (MycoAlertTM Mycoplasma Detection Kit, Lonza AG, Basel, Switzerland). Cells were cultured in monolayer at 37 °C in a

5% CO_2-containing humidified atmosphere in Dulbecco's modified Eagle's medium (DMEM), in M199 medium supplemented with 20% FBS, 100 mg/mL endothelial cell growth supplement, 50 IU/mL heparin, 100 IU/mL penicillin, and 100 mg/mL streptomycin (all from ThermoFischer Scientific, Switzerland).

Cell viability tests

HUVECs were incubated with the nanoparticles in the culture medium at different concentrations (ranging from 5 to 150 µg/ml) and for various time ranges (from 1 h to 2 days) at 37 °C. Then, the cell viability was estimated by the mitochondria-dependent reduction of MTT to formazan. After labeling, 2.0×10^4 cells/well were seeded in 48-well plates. 24 h later, cells were incubated with 1 mL/well of MTT (0.5 mg/mL) at 37 °C. Approximately 4 to 6 h were required to produce formazan; supernatants were discarded and formazan was then dissolved in DMSO. The solutions were transferred to a 96-well plate and the extent of MTT reduction to formazan within the cells was quantified by measurement of the optical density at 550 nm. Results are expressed as a percentage of the respective control (incubation in medium in the absence of nanoparticles). Duplicate measurements were performed in three independent experiments.

Acknowledgements

This research project was funded by CNRS, Unistra and the European Regional Development Fund (ERDF) in the framework of the INTERREG V Upper Rhine program ñTranscending borders with every projectò, project NANOTRANSMED.

Keywords: dendron Åsurface coating Åantifouling Åiron oxide nanoparticles Åmicrobubble

[1] T. Shryock, *Medical Economics*, **2018**, *95*, 12.
[2] A. P. Nikalje, *Med. chem.* **2015**, *5*(2), 81-89.
[3] V. V. Popov, G. Muller-Kamskii, A. Kovalevsky, G. Dzhenzhera, E. Strokin, A. Kolomiets, J. Ramon, *Biomed. Eng. Lett.* **2018**, *8*, 337-344.
[4] M. Orth, M. Averina, S. Chatzipanagiotou, G. Faure, A. Haushofer, V. Kusec, A. Machado, S. A Misbah, W. Oosterhuis, K. Pulkki, P. J. Twomey, E. Wieland, *J. Clin. Pathol.* **2019**, *72*, 191-197.
[5] J. D. Schiffman, P. G. Fisher, P. Gibbs, *Am. Soc. Clin. Oncol. Educ. Book.* **2015**, 57-65.
[6] P. Dong, K.P. Rakesh, H. M. Manukumar, Y. Hussein, E. Mohammed, C.S. Karthik, S. Sumathi, P. Mallu, H.-L. Qin, *Bioorganic Chemistry,* **2019**, *85*, 325-336.
[7] I. Martin, M. Jakob, D.J. Schaefer, *EBioMedicine* **2018**, *28*, 11-12.
[8] D. Kim, K. Shin, S. G. Kwon, T. Hyeon, *Adv.Mater.* **2018**, *30*, 1802309.
[9] P. Choudhury, M. Gupta, *Curr. Radiopharm.* **2017**, *10*(3), 166-170.
[10] Z. Jia, P. Xiu, Sl. Roohani-Esfahani, H. Zreiqat, P. Xiong, W. Zhou, J. Yan, Y. Cheng, Y. Zheng, *ACS Applied Materials & Interfaces*, **2019**, *11*(4), 4447-4469.
[11] C. R. Arciola, D. Campoccia, L. Montanaro, *Nature Reviews Microbiology*, **2018**, *16*, pages397-409.
[12] D. Van Haute, A. T. Liu, J. M. Berlin, *ACS Nano*, **2018**, *12* (1), 117-127.
[13] O. C. J. Andrén, T. Ingverud, D. Hult, J. Håkansson, Y. Bogestål, J. S. Caous, K. Blom, Y. Zhang, T. Andersson, E. Pedersen, C. Björn, P. Löwenhielm, M. Malkoch, *Adv. Healthcare Mater.* **2019**, *8*, 1801619.
[14] A. Garofalo, A. Parat, C. Bordeianu, C. Ghobril, M. Kueny-Stotz, A. Walter, J. Jouhannaud, S. Begin-Colin, D. Felder-Flesch, *New J. Chem.* **2014**, *38*, 5226-5239.
[15] D. W. Grainger, *Nature Biotechnology* **2013**, *31*, 507-509.
[16] H. Chouirfa, H. Bouloussa, V. Migonney, C. Falentin-Daudré, *Acta Biomater*. **2019**, *83*, 37-54.
[17] a) R. Michel, S. Pasche, M. Textor, D. G. Castner, *Langmuir* **2005**, *21*(26), 12327-12332; b) S. Schöttler, G. Becker, S. Winzen, T. Steinbach, K. Mohr, K. Landfester, V. Mailänder, F. R. Wurm, *Nature Nanotechnology* **2016**, *11*, 372-377.
[18] T. Alphazan, L. Mathey, M. Schwarzwälder, T.-H. Lin, A. J. Rossini, R. Wischert, V. Enyedi, H. Fontaine, M. Veillerot, A. Lesage, L. Emsley, L. Veyre, F. Martin, C. Thieuleux, C. Copéret, *Chem. Mater.* **2016**, *28*(11), 3634-3640.
[19] J. J. Giner-Casares, M. Henriksen-Lacey, M. Coronado-Puchau, L. M. Liz-Marzán, *Materials Today*, **2016**, *19*(1), 19-28.
[20] C. Bordeianu, A. Parat, S. Piant, A. Walter, C. Zbaraszczuk-Affolter, F. Meyer, S. Begin-Colin, S. Boutry, R. N. Muller, E. Jouberton, J.-M. Chezal, B. Labeille, E. Cinotti, J.-L. Perrot, E. Miot-Noirault, S. Laurent, D. Felder-Flesch, *Molecular pharmaceutics*, **2018**, *15*, 536-547.
[21] C. Bordeianu, A. Parat, C. Affolter-Zbaraszczuk, R. N. Muller, S. Boutry, S. Begin-Colin, F. Meyer, S. Laurent, D. Felder-Flesch, *J. Mater. Chem. B*, **2017**, *5*, 5152-5164.
[22] A. Cervadoro, C. Giverso, R. Pande, S. Sarangi, L. Preziosi, J. Wosik, A. Brazdeikis, P. Decuzzi, *PLoS ONE*, **2013**, *8*(2), e57332.
[23] Y. Yuan, Y. He, R. Bo, Z. Ma, Z. Wang, L. Dong, T.-Y. Lin, X. Xue, Y. Li, *Nanoscale*, **2018**, *10*, 21634-21639.
[24] A. Casset, J. Jouhannaud, A. Garofalo, C. Spiegelhalter, D.-V.Nguyen, D. Felder-Flesch, G. Pourroy, F. Pons, *Int. J. Pharmaceutics* **2019**, *556*, 287-300.
[25] R. Jahanban-Esfahlan, M. de la Guardia, D. Ahmadi, B. Yousefi, *J. Cell. Physiol.* **2018**, *233*(3), 2019-2031.
[26] X. Zheng, X. Wang, H. Mao, W. Wu, B. Liu, X. Jiang, *Nature Communications* **2015**, *6*, 5834.
[27] S. Kizaka-Kondoh, H. Konse-Nagasawa, *Cancer Science*, **2009**, *100*(8), 1366-1373
[28] J. Lau, K.-S. Lin, F. Bénard, *Theranostics* **2017**, *7*(17), 4322-4339.
[29] A. Walter, C. Billotey, A. Garofalo, C. Ulhaq-Bouillet, C. Lefèvre, J. Taleb, S. Laurent, L. Vander Elst, R. N. Muller, L. Lartigue, F. Gazeau, D. Felder-Flesch, S. Begin-Colin, *Chem. Mater.* **2014**, *26*, 5252-5264.
[30] W. K. Chong, V. Papadopoulou, P. A. Dayton, *Abdom. Radiol.* **2018,** *43*, 762-772.
[31] a) A. Jain, A. Tiwari, A. Verma, S. K. Jain, *Drug Deliv. Transl. Res.* **2018**, 8, 150-164; b) S. Wang, J. A. Hossack, A. L. Klibanov, *J. Drug. Target.* **2018**, *26*, 420-434
[32] K. H. Song, B. K. Harvey, M. A. Borden, *Theranostics*, **2018**, *8*, 4393-4408; M. S. Aw, L. Paniwnyk, D. Losic, *Exp. Opin. Drug. Deliv.* **2016**, *13*, 1383-1396.
[33] a) P. N. Nguyen, G. Nikolova, P. Polavarapu, G. Waton, L. TL Phuoc, G. Pourroy, M. P. Krafft, *RSC Adv*. **2013**, *3*, 7743-7746; b) A. Kovalenko, P. Polavarapu, M. P. Krafft, G. Waton, G. Pourroy, *Soft Matter*, **2014**, *10*, 5147-356; c) J. C. Owen, C. Crake, D. Carugo, E. Beguin, A. A. Khrapitchev, R. J. Browning, N. Sibson, E. Stride, *Drug. Deliv. Transl. Res.* **2018**, *8*, 342-152.
[34] L. Fass, *Mol. Oncol.* **2008**, *2*, 115-152.
[35] G. Sauerbrey, *Z. Phys.* **1959**,*155*, 206-222.

FULL PAPER

Dendritic phosphonates are versatile coatings of several nanomaterials for health applications ranging from implants to nanoparticles and microbubbles

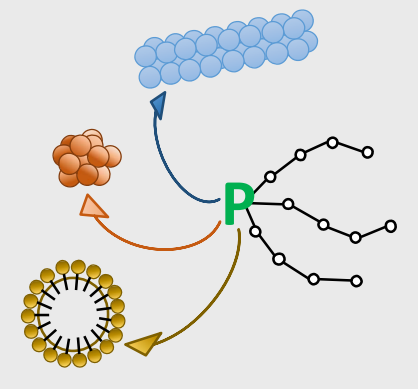

*Dinh-Vu Nguyen, Ludivine Hugoni, Miriam Filippi, Francis Perton, Da Shi, Emilie Voirin, Laura Power, Geoffrey Cotin, Marie -Pierre Krafft, Arnaud Scherberich, Philippe Lavalle, Sylvie Begin-Colin and Delphine Felder-Flesch**

Page No. ï Page No.

Mastering bioactive coatings of metal oxide nanoparticles and surfaces through phosphonate dendrons